2013

Airbreathing rotating detonation wave engine cycle analysis

Eric M. Braun
University of Texas at Arlington

Frank K. Lu
University of Texas at Arlington

Donald R. Wilson
University of Texas at Arlington

Jose A. Camberos
U.S. Air Force Research Laboratory

Aerospace Science and Technology 27 (2013) 201–208

Contents lists available at SciVerse ScienceDirect

Aerospace Science and Technology

www.elsevier.com/locate/aescte

Airbreathing rotating detonation wave engine cycle analysis ☆

Eric M. Braun [a,*], Frank K. Lu [a], Donald R. Wilson [a], José A. Camberos [b]

[a] University of Texas at Arlington, Arlington, TX 76019, USA
[b] U.S. Air Force Research Laboratory, Wright-Patterson Air Force Base, OH 45433, USA

ARTICLE INFO

Article history:
Received 24 November 2010
Received in revised form 7 July 2012
Accepted 25 August 2012
Available online 29 August 2012

Keywords:
Detonation
Cycle analysis
Propulsion system

ABSTRACT

A cycle analysis model for an airbreathing, rotating detonation wave engine (RDE) is presented. The engine consists of a steady inlet system with an isolator which delivers air into an annular combustor. A detonation wave continuously rotates around the combustor with side relief as the flow expands towards the nozzle. A model for the side relief is used to find the pressure distribution around the combustor. Air and fuel enter the combustor when the rarefaction wave pressure behind the detonation front drops to the inlet supply pressure. To create a stable RDE, the inlet pressure is matched in a convergence process with the average combustor pressure by increasing the annulus channel radial width with respect to the isolator channel. Performance of this engine is considered using several parametric studies and compared with rocket-mode computational results. A hydrogen–air RDE reaches a specific impulse of 3800 s and can reach a flight speed of Mach 5.

1. Introduction

Detonation-based engines have been studied in recent decades because of their potential for improved efficiency over Brayton cycle engines [16,30,33]. The well-known pulsed detonation engine (PDE) is characterized by an unsteady cycle composed of filling a combustor tube with a reactive mixture, closing one end and igniting the mixture to initiate a detonation wave. Thrust production occurs as the gas exhausts from the tube, after which filling will begin again. Many challenges exist for implementing the unsteady cycle of a PDE with a steady inlet and nozzle for airbreathing flight. For hypersonic flight, the oblique detonation wave engine (ODWE) has been studied since a detonation wave can be stabilized inside a combustor with a sufficiently high entrance velocity [32]. Engines with these cycles integrated into several flight speed domains have been proposed as part of hybrid configurations [21,22].

Another variant called the rotating detonation wave engine (RDE) consists of a detonation wave continuously rotating around an annular combustor that is sustained by axial injection of fresh reactants from one end. Continuous axial injection produces a triangular region of fresh reactants that penetrates into the combustor between wave fronts. The penetration distance, referred to as the fresh mixture layer height h_m, is a key factor in RDE design. The detonation wave front can only exist up to this height, after which the combustion products are free to expand on one side. These expanding products interact with the products from the previous rotation, and the resulting flow field has been called a detonation-shock combined wave [11,38]. A detailed review of the physical processes behind the RDE is presented by Bykovskii et al. [4]. The RDE may also operate with steady state inlet and exit flow conditions since the rotational frequency of the detonation wave traveling in the annulus is 1–10 kHz.

Initial RDE studies were conducted by Voitsekhovskii [39] and Nicholls et al. [27] in the early 1960s. Recent computational efforts have shown that stable RDE combustor flow can be realized with high efficiency [15,29,34,41]. Experimental studies have demonstrated that it can be operated for a wide variety of fuels and injection conditions [5,7,19]. Despite these achievements, engine tests are limited to a few seconds or less while factors like heating, injector dynamics, mixing, detonation–turbulence interaction [24], and the effects of curved channels [25] are topics of current investigation.

A range of injection strategies and combustor entrance velocities appear feasible [10]. Fuel injection in rocket-mode simulations is controlled by arrays of sonic micronozzles connected to a plenum chamber with a specified total pressure [41]. The rise in pressure from the detonation wave temporarily shuts off a portion of the injector orifices, but refueling begins when the pressure behind the wave reduces below that of the plenum chamber. Experiments by Canteins and Kindracki et al. have shown that these orifice arrays can be substituted with narrow slits [7,19]. Zhdan has shown in a computational model that the rotating detonation wave can be stabilized for incoming supersonic reactant flow [42]. This RDE model consisted of a cylindrical channel with

☆ A version of this article was presented as AIAA paper 2010-7039 at the 46th AIAA/ASME/SAE/ASEE Joint Propulsion Conference & Exhibit, Nashville, Tennessee, July 25–28, 2010.

* Corresponding author. Tel.: +1 817 272 5120; fax: +1 817 272 5124.
E-mail address: eric.braun@mavs.uta.edu (E.M. Braun).

1270-9638/$ – see front matter
http://dx.doi.org/10.1016/j.ast.2012.08.010

Nomenclature

A	Area	m^2	
B	Annulus entrance blockage factor		
C	Annulus circumference	m	
CJ	Chapman–Jouguet state		
c_p	Specific heat at constant pressure	J/(kg K)	
d	Annulus diameter	m	
f	Fuel/air mass flow rate ratio		
$F/\dot{m}_o$	Specific thrust	N/(kg/s)	
h	Specific static enthalpy	J/kg	
h_m	Annulus fresh mixture height	m	
I_{sp}	Specific impulse	s	
M	Mach number		
p	Static pressure	Pa	
q	Dynamic pressure	Pa	
r	Distance behind wave front	m	
R	Gas constant	J/(kg K)	
s	Specific entropy	J/(kg K)	
Sa	Stream thrust	N/(kg/s)	
t	Time	s	
T	Temperature	K	
V	Velocity	m/s	
V_{an}	Annulus axial entrance velocity	m/s	
ZND	Zel'dovich–von Neumann–Döring state		
Δ_1	Isolator channel initial radial width	m	
Δ_2	Isolator channel final radial width	m	
Δ_3	Detonation channel radial width	m	
ϕ	Equivalence ratio		
γ	Specific heat ratio		
η_c	Compression efficiency		
η_e	Nozzle efficiency		
λ	Detonation cell size	m	
ρ	Density	kg/m^3	
τ	Annulus wave period, $= \tau_F + \tau_D$	s	
τ_D	Detonation time	s	
τ_F	Refilling time	s	
Ψ	Cycle static temperature ratio		

Subscripts

0	Freestream property
t	Stagnation property

axial inflow at a specified Mach number before the area increased to a larger channel where the detonation wave continuously propagated.

The flexibility of the RDE combustor means potential exists for integration into a high-speed airbreathing engine. In this study, cycle analysis of an airbreathing RDE has been developed to determine performance results and critical trends. Since the RDE can operate with a steady-state inlet and nozzle due to the high rotational frequency of the wave, the model is quasi-one-dimensional and time independent. The combustor is associated with an operating frequency which is the annulus circumference divided by the detonation wave speed. The fresh mixture layer height h_m is dependent on this frequency and the combustor entrance velocity. In the combustor, gas properties are primarily dependent on the annulus circumference, entrance velocity, and detonation wave speed. Ultimately, h_m is determined using an iterative solution. The combustion products expand toward the nozzle in the detonation-blast combined wave system. Expansion is modeled as a function of distance behind the wave front and a pressure distribution around the circumference of the combustor is created. Similar to computational studies, fresh mixture injection is blocked where the detonation wave pressure exceeds the refueling pressure. This blockage ratio, also determined using an iterative solution, is constant for a particular operating condition. The constant blockage ratio for fresh flow into the annulus along with the expanding products behind the wave produces uniform outlet flow. Although the annulus pressure at a fixed point can be displayed as a function of time since a detonation wave speed is associated with the combustor, the model is essentially one-dimensional.

Instead of a plenum chamber, an isolator similar to the computational work of Zhdan [42] is used for this model. Unlike a PDE, no mechanical systems operate fast enough to counteract the pressure gain of an RDE. Zhdan increased the channel radial width by a factor of 2 as the supersonic flow entered the combustor. The expansion counteracts pressure gain and stabilizes the wave. The channel radial width increase is variable for the current model. Again, the final areas are determined using an iterative solution where convergence is obtained when the averaged static pressure in the combustion annulus matches the pressure of the incoming flow in the isolator. A real gas model with adiabatic process efficiencies has been used to calculate gas properties at each engine stage.

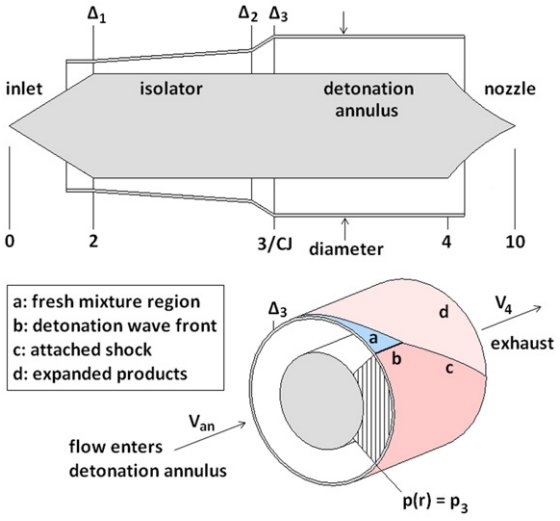

Fig. 1. Basic engine geometry and stage designations (not to scale).

2. Analysis procedure

The subsections contained in this section follow the cycle analysis model. The real gas model uses the chemical kinetics program Cantera [12] to calculate the thermodynamic properties at each engine stage. The kinetic mechanism GRI-Mech 3.0 [37], which contains 53 species and 325 reactions validated with experimental data, is utilized for fuel–air detonation. Details of the numerical detonation solutions and validation are presented in Browne et al. [2]. The fuels used in the current work are hydrogen ($2H_2 + O_2 + 3.76N_2$) and propane ($C_3H_8 + 5O_2 + 18.8N_2$).

2.1. Initial conditions and sizing

The initial conditions for the analysis are the flight parameters M_0, p_0, and T_0. Fig. 1 shows a cutaway view of the engine with geometry and staging labeled. Fig. 2 depicts the unwrapped

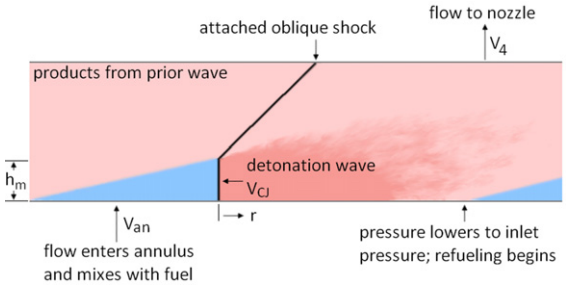

Fig. 2. Schematic of the rotating detonation wave structure.

Table 1
Minimum RDE diameter estimates.

Mixture contents ($\phi = 1$)	λ (mm)	h_m (m)	d_{min} (m)
$2H_2 + O_2$	1.4	0.017	0.042
$2H_2$ + air	15.1	0.181	0.453
$C_3H_8 + 5O_2$	1.5	0.018	0.045
C_3H_8 + 5(air)	52.5	0.63	1.575

flow in the combustor annulus. Two geometric properties that are held constant while the analysis is conducted are the diameter of the annulus d and the combustor channel radial width Δ_3. Values of the isolator channel radial width Δ_2 and h_m are initialized for the iterative solution. Note that the increase from Δ_2 to Δ_3 assumes an isentropic expansion which will necessitate appropriate contouring yet to be experimentally determined. Where Δ_2 is labeled in Fig. 1, part of the channel is blocked where the pressure from the detonation wave exceeds that of the inlet. The annulus entrance blockage factor B accounts for the fraction of the isolator flow in the area defined by Δ_2 that can expand to the Δ_3 area. To maintain constant flow properties, the isolator must increase in radial width from Δ_1 to Δ_2 where the area created with d and Δ_1 is equal to the area created with d and Δ_2 multiplied by B. The freestream flow and inlet are labeled as stages 0 and 2, respectively. The unblocked flow that expands into the annulus prior to detonation is labeled stage 3. Stage CJ accounts for the combustion temperature at the detonation wave front, then followed by expansion of the products. Labeled as stage 4, the properties of the products from the pressure distribution that is modeled are averaged to account for attenuation of the wave that occurs at the end of the annulus. The nozzle properties are labeled as stage 10. In Fig. 2, h_m is labeled along with a depiction of the triangular fresh mixture layer region, the detonation wave front, and the attached shock.

Thus far, the sizing of the RDE has been based on a set of minimum empirical standards outlined by Bykovskii et al. [4]. The minimum axial mixing length h_m for a stable RDE is $(12 \pm 5)\lambda$, where λ is the detonation cell width. The minimum diameter and channel radial width are estimated to be $d = 30\lambda$ and $\Delta_3 = 2.5\lambda$, respectively. Physically, these requirements are due to the presence of transverse waves in the detonation front which destabilize around tight curves and in narrow channels. The transverse wave spacing is related to the reaction zone width of the detonation wave, and tracking the triple points formed between them and the leading shock in time reveals a pattern of diamond shaped cells. The ratio of h_m/C for is also estimated by Bykovskii et al. to be 0.14 ± 0.04 for gaseous fuels and oxidizers. Using cell size data for fuel–oxidizer mixtures at standard atmospheric conditions [13,17,18,20,23], RDE diameter estimates are shown in Table 1. The cell width of the propane–air mixture, similar to many hydrocarbon–air mixtures, equates with a minimum diameter of 1.6 m. However, λ decreases as pressure and temperature increase so the engine could be smaller depending on the combustor entrance conditions. The fuel–air engine diameters in Table 1 are held constant for this study. The effect of the centrifugal force was considered [26], but a preliminary investigation with the combustor flow conditions and geometry showed that it makes a negligible impact on performance. Consequently, Δ_3/d was fixed at 0.1 which ensures stability according to the empirical estimates. Increasing Δ_3 can lead to a higher power density for an engine of diameter d, but varying it in this study has no impact on performance indicators like specific impulse which are independent of area.

2.2. Inlet and isolator

The inlet system properties are calculated as a function of $\Psi = T_2/T_0$ using an analysis procedure outlined in Ref. [14] that has been expanded for a real gas model. Values for p_2, A_{Δ_1}/A_0, and M_2 are determined before moving to the next stage. Since ram compression is assumed for this model, adiabatic process efficiencies based on static enthalpy have been utilized where $\eta_c = (h_2 - h_{2x})/(h_2 - h_0)$. At stage 2x, $s_{2x} = s_2$ and $p_{2x} = p_0$. The efficiency definition, Gibbs equation, and energy equation can be used to find the following properties:

$$T_{2x} = \left(\frac{c_{p,0}T_0}{c_{p,2x}}\right)\left[\frac{c_{p,2}}{c_{p,0}}\Psi + \eta_c\left(1 - \frac{c_{p,2}\Psi}{c_{p,0}}\right)\right] \tag{1}$$

$$V_{2x} = \sqrt{{V_0}^2 - 2c_{p,0}T_0\left[\frac{c_{p,2}\Psi}{c_{p,0}}(1-\eta_c) + \eta_c - 1\right]} \tag{2}$$

In Eqs. (1) and (2), a value for $c_{p,2}$ is initiated and converged upon using an iterative process with the resulting real gas model properties. Since stage 2 has equivalent stagnation enthalpy to stage 2x, the Mach number M_2 can be determined.

$$M_2 = \sqrt{\frac{2(h_{t,2x} - c_{p,2}T_2)}{\gamma_2 R_2 T_2}} \tag{3}$$

The static pressure p_2 is found using an iterative process that determines s_2 with the known temperature T_2 until $s_2 = s_{2x}$. With p_2 and T_2 input into the real gas model program, all of the other static properties are known. The stagnation temperature and pressure are determined while accounting for the variation in specific heat from the static to the stagnation states. An additional solution process determines

$$T_{t,2} = \frac{(c_{p,2}T_2 + {V_2}^2/2)}{c_{p,t2}} \tag{4}$$

$$p_{t,2} = p_2\left[\frac{T_{t,2}}{T_2}\right]^{(c_{p,2}+c_{p,t2})/(2R_2)} \tag{5}$$

where $c_{p,t2}$ is iterated using entropy as a convergence criterion. Note that Eq. (5) is an approximation that assumes an average value of c_p from the static to stagnation states. Minimal error is incurred from this approximation so long as M_2 is below the hypersonic regime (< 5 in this study) and, additionally, $T_2 < 800$ K to prevent autoignition in the combustor.

The isolator properties are constant at its beginning and end as the area expands because of the blockage from the detonation wave ($A_{\Delta_1} = BA_{\Delta_2}$). For the isolator and average annulus pressures to match during combustion with pressure gain, $A_{\Delta_3} > A_{\Delta_2}$. Since the isolator flow is choked, expanding the area defined by Δ_2 to that defined by Δ_3 also leads to a rise in axial velocity of fresh reactants to refuel the combustor between detonation waves. The stage 3 properties are found by specifying an initial value of $A_{\Delta_2}/A_{\Delta_3}$, which will later be iterated until the isolator and average annulus properties match. This expansion is considered ideal in the current work so total enthalpy is conserved.

$$\frac{A_{\Delta_3}}{A_{\Delta_2}} = \left[\frac{d^2 - (d-\Delta_3)^2}{(d-\Delta_3+\Delta_2)^2 - (d-\Delta_3)^2}\right] \tag{6}$$

The flow is isentropic and choked with a constant mass flow rate in this expansion. Using a similar solution process described with Eqs. (4) and (5), a combination of the conservation of enthalpy and state equation yield T_3 in

$$\frac{A_{\Delta_2}}{A_{\Delta_3}} = \frac{p_{t3}}{\rho_2 V_2 R_3 T_3} \frac{\sqrt{2(h_{t2} - c_{p,3}T_3)}}{[\frac{T_{t3}}{T_3}]^{(c_{p,3}+c_{p,t3})/(2R_3)}} \tag{7}$$

After T_3 is determined, p_3 is found using an equivalent of Eq. (5). With the other static properties found using the real gas model, V_{an} is solved for using the conservation of mass. The initial estimate for Δ_2 affects the air properties prior to detonation as Δ_3 is held constant. If Δ_2 is too large, $p_4 > p_2$ and the engine is not stable. Fuel is added to the air to form a stoichiometric mixture which is detonated. Although the mixing was idealized in this study to occur with no losses, a practical fuel injector system, probably consisting of sidewall-mounted impinging injector arrays, will need to be developed. The post-detonation properties are based on the Zel'dovich–von Neumann–Döring (ZND) wave model. The model consists of a shock wave which heats the fuel–air mixture so chemical reactions occur to initiate combustion. The combustion ends at the Chapman–Jouguet state where the velocity of the wave is equivalent to the speed of sound of the combustion products [9].

2.3. Detonation wave properties in the annulus

As depicted in Fig. 2, V_{an} is the axial velocity of the fuel–air mixture as it enters the annulus at stage 3. The detonation wave properties are solved for using the numerical solution by Browne et al. [2] with p_3 and T_3 as the initial conditions. The pressure distribution along the circumference of the annulus is then determined. In Fig. 2, the term r is the distance along the annulus starting at the wave front and moving back from it. All of the property distributions are functions of r. Although rocket-mode engines have been observed to have more than one detonation wave traveling around the annulus at once, the number of waves appears to reduce when air is used instead of O_2 [4]. Accordingly, the model contains only one detonation wave. At a fixed point on the annulus for one rotation of the wave at speed V_{CJ}, the refueling time is $\tau_F = V_{an}/h_m$ and the time when the combustor pressure is higher than that of the inlet is τ_D.

A one-dimensional model for the property distributions as a function of distance behind the detonation wave in a tube is described in Ref. [8]. The rarefaction wave that follows the detonation front is self-similar. Models for the detonation-blast system with side relief have also been developed [35,36] but not specifically applied to a RDE. A notable result obtained from Ref. [36] is that the pressure reduction behind a detonation wave front of height h_m is a function of the dimensionless variable $\xi = r/h_m$. This result was obtained by a method-of-characteristics solution whereby the pressure behind the detonation front lowers with an expansion wave forming as the combustion products are expanding. The degree of expansion is controlled by a slip line between the combustion products of consecutive detonation wave fronts. The slip line angle is calculated using the Prandtl–Meyer function [1]. The angle of the oblique shock is then determined using the slip line angle as the deflection angle with a Mach number calculated from the detonation wave speed and the stage 4 gas speed of sound. An iterative solution is required to match pressures at the slip line and determine the Mach numbers. However, these angles are not required for the cycle analysis as it was then found by Sichel and Foster that $p(r)/p_{CJ}$ and ξ have an identical relationship for a variety of fuel–air mixtures. The tabulated values of $p(r)/p_{CJ}$ and ξ were implemented into the current combustor model.

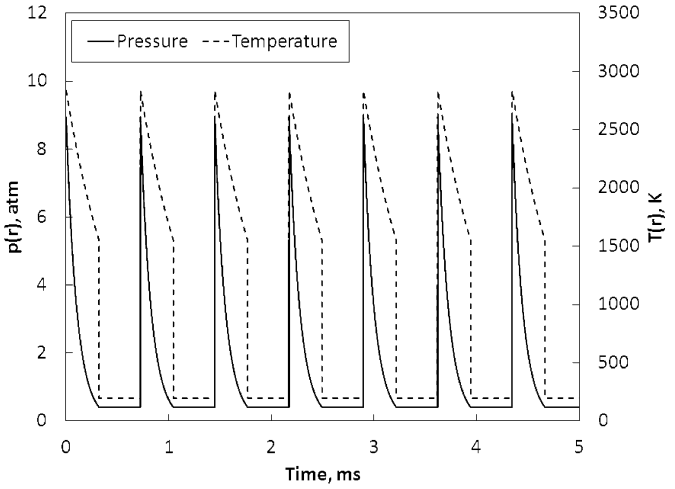

Fig. 3. Example property distributions within the RDE annulus using an H_2–air mixture.

For an isentropic expansion with a constant specific heat approximation, the temperature distribution around the annulus is calculated using:

$$T(r) = T_{CJ}\left(\frac{p(r)}{p_{CJ}}\right)^{(\gamma_{CJ}-1)/(\gamma_{CJ})} \tag{8}$$

Next, determining the location where the rarefaction wave pressure matches the injection pressure p_3 is critical for the RDE model. The rarefaction wave pressure will continue to reduce behind the detonation wave until the pressure drops to p_3. The analysis program is designed to locate this point, which is then used to update the initial estimate for the blockage value B. The pressure then remains at p_3 during filling. Fig. 3 shows a few cycles with the $p(r)$ and $T(r)$ distributions. Note that this case is an arbitrary example and time can appear on the abscissa of the graph since $dr = V_{CJ}\,dt$. The behavior of the detonation wave front has been observed and modeled by Nakayama et al. for a range of curved channel radial widths [25]. So long as the propagating detonation wave is stable, its velocity does not change significantly across the radial width of the curved channel such that the flow field would resemble Couette flow. Although the velocity indeed reduces slightly along the inner wall, it was assumed that the velocity is constant in this model.

2.4. Annulus exit conditions

According to Bykovskii et al., the optimum length of the annulus should be about $4h_m$ [4]. The attached oblique shock in the combustor attenuates at the end of the annulus as seen in computational results [15,34,41]. For modeling purposes, it is then sufficient to assume that the pressure and temperature distributions can be averaged at the end of the annulus before being exhausted through a nozzle. More specifically, p_4 is the mean value of the pressure distribution around the annulus while T_4 is calculated using Eq. (9) which uses an average c_p for the expansion. The process is isentropic, and an iterative solution is used where $c_{p,4}$ is determined using a convergence criterion of $s_{CJ} = s_4$.

$$T_4 = T_{CJ}\left(\frac{p_4}{P_{CJ}}\right)^{(2R_{CJ}/(c_{p,CJ}+c_{p,4}))} \tag{9}$$

The exit flow velocity is primarily axial although a radial component indeed exists [15]. Assuming that total enthalpy is conserved from the detonation wave front to the exit leads to unrealistically high exit velocity and performance predictions. The constant channel radial width, rocket-mode RDE model by Bykovskii et al. is considered thermally choked at the exit with a Mach number of 1.0 [4]. Fixing the exit Mach number to 1.0 has resulted in a useful model for performance predictions. However, the computational RDE combustors detailed in recent research have an exit Mach number above 1.0 [15,34,41], so fixing the exit Mach number at 1.0 underestimates performance. The model used to calculate the exit velocity in the current work is based on the study by Nordeen et al. where the work required to turn the flow in the combustor must be accounted for with a total enthalpy loss using the Euler pump equation and rothalpy [28]. The analysis approach by Nordeen et al. can be written in several forms, and it has been verified with computational RDE results.

$$c_{p,\mathrm{CJ}}T_{\mathrm{CJ}} + \frac{{V_{an}}^2}{2} - V_{an}\cdot V_{\mathrm{CJ}} = c_{p,4}T_{t,4} - V_{4,x}\cdot V_{4,z} \tag{10}$$

In Eq. (10), $T_{t,4}$ is solved for using the detonation wave properties and a value of V_4 that is found from the conservation of mass relationship for the flow entering the detonation wave front area ($\Delta_2 h_m$) which must be equivalent to the flow exiting the constant area combustor. Note that V_4 is also split into axial and radial components required for the flow turning work analysis. For the current work, $V_{4,z}$ is estimated using Eq. (11) from Ref. [8] which is a one-dimensional velocity distribution based on distance behind the detonation front. Alternatively, a value for $V_{4,z}$ could be assigned as a percentage of V_4. Both $V_{4,z}$ calculation approaches result in minimal changes to overall performance.

$$V_{4,z}(r) = V_{\mathrm{CJ}} - \frac{2}{\gamma_{\mathrm{CJ}}+1}\left[\frac{r}{C/V_{\mathrm{CJ}} - t(r)}\right] \tag{11}$$

Using this analysis, the exit Mach number for the annulus is 1.0–1.3 for the parametric studies covered in the upcoming results. Once the stage 4 properties are determined, the estimate for Δ_2 is iterated. The requirement for convergence of the isolator channel radial width is that the pressure p_2 must be equal to the averaged annulus pressure p_4.

2.5. Nozzle and performance parameters

Nozzle equations with process efficiencies again based on static enthalpy are used for the expansion process through what will likely be an annular aerospike nozzle. At stage 2y, $p_{10\mathrm{y}} = p_0$ and $T_{10\mathrm{y}}$ can be determined since the process is isentropic and $S_{10\mathrm{y}} = S_4$. The adiabatic process efficiency is $\eta_e = (h_4 - h_{10})/(h_4 - h_{4\mathrm{y}})$. At stage 10, $p_{10} = p_0$ and an iterative solution that converges on a value for $c_{p,10}$ can be used to find T_{10}.

$$T_{10} = \frac{c_{p,4}T_4}{c_{p,10}}\left[1 - \eta_e\left(1 - \frac{c_{p,10\mathrm{y}}T_{10\mathrm{y}}}{c_{p,4}T_4}\right)\right] \tag{12}$$

The stage 10 static temperature and pressure are then input into the real gas model to find the other gas properties. Stagnation properties can then be determined using analogs to Eqs. (4) and (5) for an expansion.

A stream thrust analysis was used for the specific thrust performance prediction where $Sa = V(1 + RT/V^2)$ at each stage [14]. Note that specific impulse I_{sp} is the specific thrust in Eq. (14) divided by the product of f and the gravity constant.

$$\frac{A_{10}}{A_0} = \left(\Psi\frac{p_0}{p_2}\frac{V_0}{V_2}\right)\left(\frac{A_3}{A_1}\right)\left[(1+f)\frac{T_{10}}{T_4}\frac{p_4}{p_{10}}\frac{V_4}{V_{10}}\right] \tag{13}$$

$$\frac{F}{\dot{m}_0} = (1+f)Sa_{10} - Sa_0 - \frac{R_0T_0}{V_0}\left(\frac{A_{10}}{A_0} - 1\right) \tag{14}$$

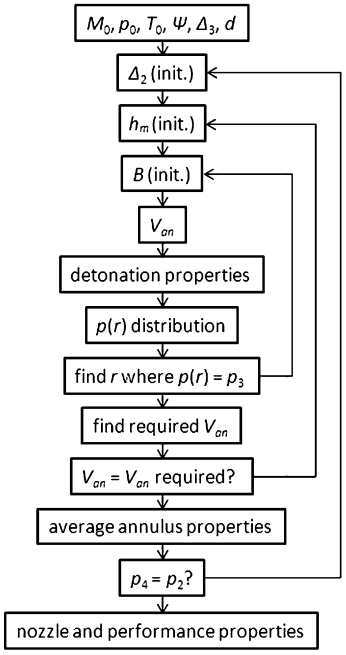

Fig. 4. Summary of the RDE cycle analysis procedure.

Depending on the initial conditions, the computation time for a test case in a MATLAB environment is on the order of a few minutes or less with a single processor computer.

2.6. Summary

Fig. 4 provides a summary of the RDE cycle analysis procedure. Using initial estimates of Δ_2, h_m, and B, the pressure distribution around the annulus is calculated. The value of B is iterated until it correctly matches with r/C where $p(r) = p_3$. With an estimate for h_m, the speed of the detonation wave can be used to calculate a required annulus entrance velocity to compare to V_{an}. If the two values are not equivalent, h_m is either increased or decreased. The height h_m, inlet gas velocity, and detonation wave velocity are related by $V_{an} = h_m/\tau_F = BC/V_{\mathrm{CJ}}$. Finally, the condition where p_4 must be equal to p_2 is met by iterating Δ_2 to change p_3 prior to detonation.

3. Performance results

3.1. CFD comparison

With a few minor modifications, the thrust and specific impulse can be compared to the work of Yi et al. [41]. Yi et al. reported specific impulse and thrust at a flight speed of Mach 1.5 and plenum chamber conditions of $p_0 = 7$–15 atm and $T_0 = 500$ K. Sonic micronozzle injectors were used. An area ratio of the combined nozzle throats and combustion annulus was specified as 0.4. The boundary conditions of this airbreathing RDE model were changed to these stagnation conditions with $M_2 = 1.0$ in the isolator. The area ratio of the isolator channel Δ_2 to the combustion annulus channel Δ_3 was fixed at 0.4. Fixing the area ratio means that $p_2 > p_4$, which is physically realistic for a rocket-mode RDE. Fig. 5 shows the results of the comparison. The specific impulse and thrust were not expected to match exactly, but they are similar over the stagnation pressure range used. More importantly, the specific impulse shows a slight increase with stagnation pressure while the thrust increases linearly for each model. Note that specific thrust is reported in kN per the annulus channel radial width Δ_3.

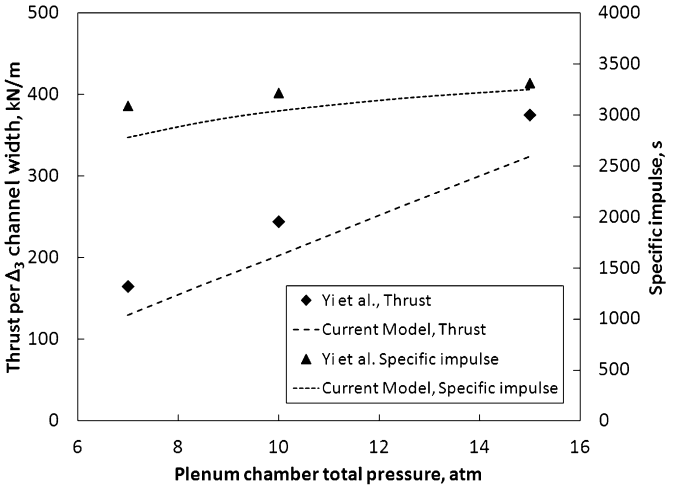

Fig. 5. Performance comparison with the computational model by Yi et al. at a Mach 1.5 flight speed [41].

3.2. Ideal H_2–air engine

Fig. 6 maps the theoretical performance of the ideal, H_2–air RDE with a dynamic pressure q_0 of 95 kN/m^2. The H_2–air mixture is stoichiometric at all times in the study ($\phi = 1.0$, $f = 0.0293$). As would be expected, specific impulse and thrust increase with cycle static temperature ratio. Specific impulse reaches about 3800 s at a Mach 1.5 flight speed. A flight Mach number of 5 is reached before autoignition of the mixture occurs, which would prevent the detonation wave from forming. Note that $T_0\Psi$ in Fig. 6(a) is above the H_2–air autoignition temperature of 750 K because it is calculated with T_2 before the flow expands into the annulus where the temperature lowers slightly to T_3.

Not every case plotted in Fig. 6(a) is physically reasonable, so the additional dashed lines appearing on the graph are boundaries. First, Ψ is limited to keep the isolator flow supersonic, leading to an increase in velocity and a decrease in static pressure as it enters the annulus. Subsonic flow into the annulus first experiences a large reduction in h_m to the point where stability of the rotating detonation wave cannot be guaranteed. An area expansion with subsonic flow also results in a static pressure increase, which works against the need to decrease p_3 so $p_4 = p_2$. Zhdan has shown an entrance velocity above Mach 3 generally leads to a condition where the incoming flow speed becomes comparable to the rotating wave structure, thereby causing it to destabilize [42]. Consequently, the light dashed line indicates an entrance velocity of $M_3 = 3.0$ to serve as an estimate where the RDE may become unstable. These boundaries lead to a region of physically reasonable design space where the RDE can operate in. As shown in Fig. 6(b), the annulus-to-isolator area ratio plays a significant role in the overall RDE performance. High area ratios negatively impact performance because they indicate that p_3 is lowering and less overall thrust work is created. The maximum specific impulse reached while the isolator flow reaches $M_2 = 1$ gradually lowers with Mach number. This gradual decrease has been predicted for supersonic, airbreathing detonation-based engines [3].

The minimum height requirement for the incoming mixture is met within the stability requirements of Bykovskii et al. [4] and continues to increase with M_0. The blockage factor B at $\Psi = 1$ ranges from 0.5–0.25 for flight speeds of Mach 1.5–5.0 and 0.5–0.6 for the maximum Ψ values over the same Mach number range. Although p_4/p_0 is fairly low when $M_0 < 2$, it increases rapidly with Ψ. For instance, $p_4/p_0 = 9.0$ for $M_0 = 2.5$ and $\Psi = 1.85$. The Reynolds number of the flow exiting the combustor (stage 4) is 1–2 million/m for Mach 1.5 and 1.5–15 million/m for Mach 5.

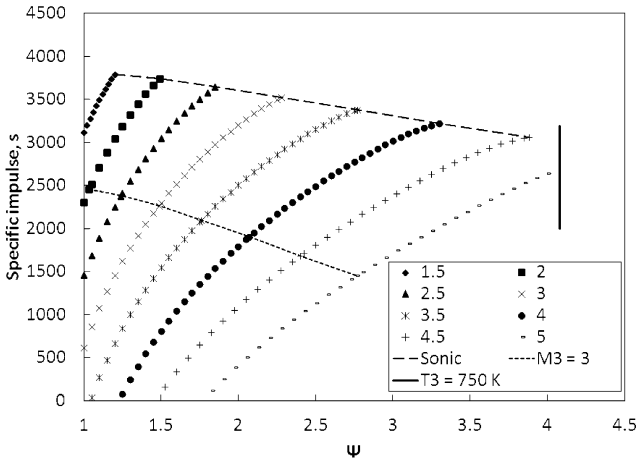

(a) Specific impulse.

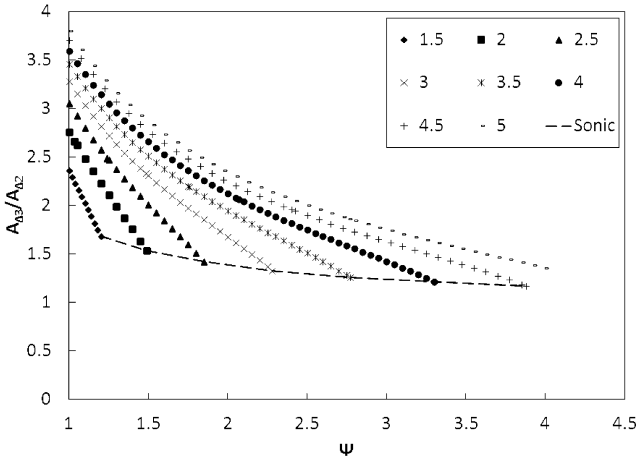

(b) Annulus-to-isolator area ratio.

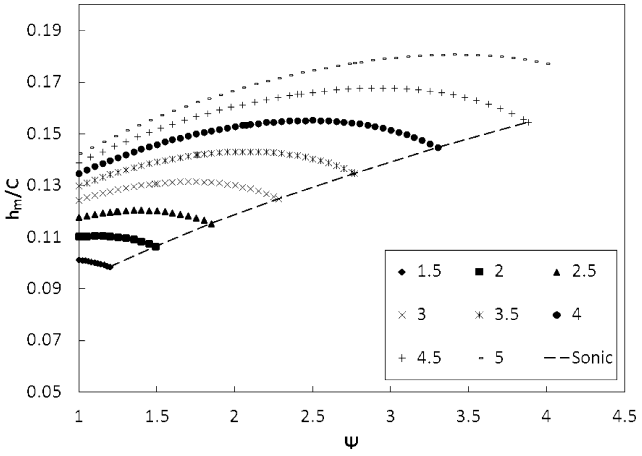

(c) Ratio of fresh mixture layer height to the annulus circumference h_m/C.

Fig. 6. Performance versus cycle static temperature ratio for an ideal RDE with $q_0 = 95$ kN/m^2, $T_0 = 216.7$ K, $d = 0.453$ m, H_2–air, and no contact surface burning. Lines of constant flight Mach number are plotted.

The airbreathing RDE can be compared with an airbreathing PDE. For the same H_2–air mixture, Wu et al. developed a PDE model that predicted specific impulse to be 3680 seconds at a flight speed of Mach 2.1 and an altitude of 9300 m [40]. Maximum RDE performance at this flight condition with the current model is 3600 s. Dissociation losses in airbreathing PDE combustors are

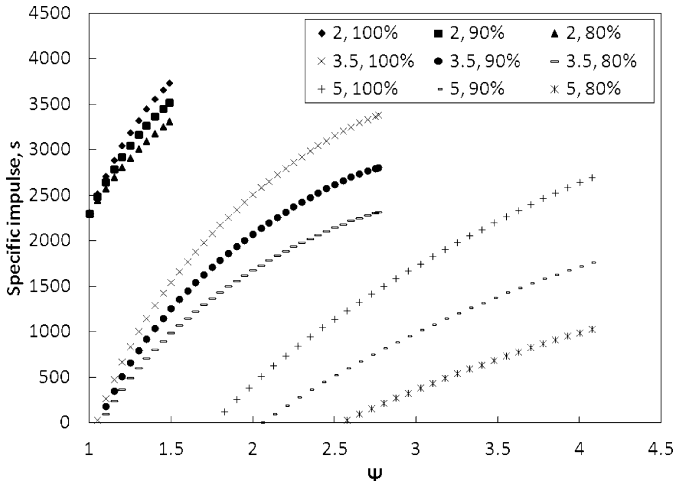

Fig. 7. Performance comparison with $\eta_c = \eta_e$ equal to 100%, 90%, and 80%.

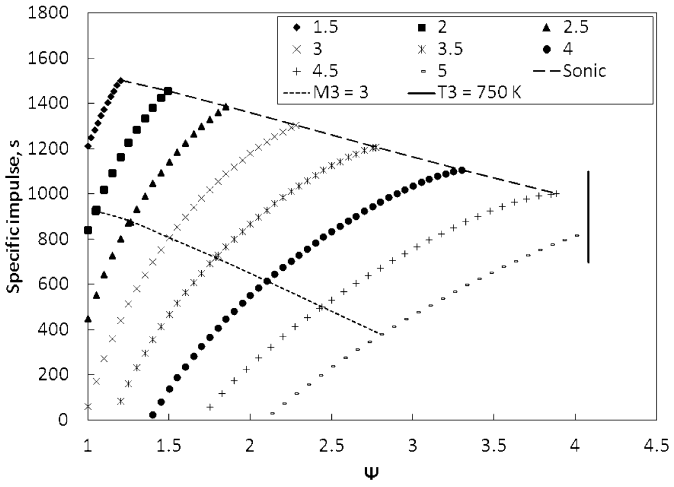

(a) Specific impulse.

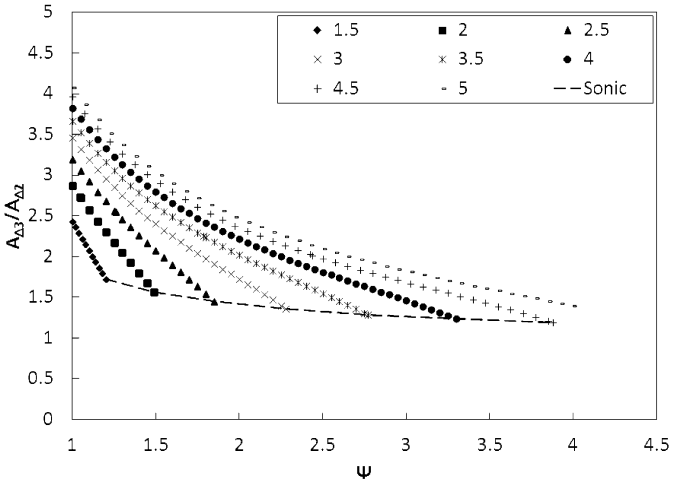

(b) Annulus-to-isolator area ratio.

Fig. 8. Performance versus cycle static temperature ratio for an ideal RDE with $q_0 = 95$ kN/m^2, $T_0 = 216.7$ K, $d = 1.575$ m, C_3H_8–air, and no contact surface burning. Lines of constant flight Mach number are plotted.

about 10% higher than Brayton cycle engines [31]. Since both engines utilize propagating detonation waves, the dissociation losses in the RDE may be expected to be similar for comparable inlet conditions. However, it should be noted that dissociation lowers V_{CJ} which, for an RDE, also lowers the required flow turning work. Future comparisons of the PDE and RDE will require an analysis approach such as optimization via entropy generation minimization [6] that can consider factors like thrust density and parasitic losses in addition to specific impulse.

3.3. Effect of component efficiency

Compression and nozzle adiabatic process efficiencies were added to the model to assess their impact on performance. In Fig. 7, ideal cases are plotted with those where η_c and η_e have been set to either 90 or 80 percent. Although the efficiency values were added in the cases for $\Psi = 1.0$, there is no difference in performance because no air is compressed and $p_0 = p_4$. As Ψ and M_0 increase, lowering the component efficiencies can significantly decrease I_{sp}. Parametric studies with dynamic pressure showed a difference of only a few percent. All the parametric efficiency studies had minimal impacts on the values for $A_{\Delta_3}/A_{\Delta_2}$ and h_m.

3.4. Ideal C_3H_8–air engine

To gain an understanding of how an airbreathing, hydrocarbon RDE may perform, propane was used as fuel ($\phi = 1.0$, $f = 0.064$) for the plots in Fig. 8 under otherwise identical initial conditions as the ideal hydrogen cases. Specific impulse can be expected to drop for two reasons. First, the lower heating value of propane is significantly less than hydrogen. Second, the CJ pressure ratio for hydrocarbon–air mixtures is higher than that for hydrogen–air mixtures. In order to match p_4 to p_2, the area ratio A_3/A_2 must increase more and lead to a greater reduction to static pressure prior to detonation. For the propane-based RDE, the maximum specific impulse at the Mach 1.5 flight condition is 1500 s. The flight speed still reaches to about Mach 5 with a corridor of feasible solution space similar to what was seen with the use of hydrogen.

4. Conclusions

The ideal airbreathing RDE model shows an I_{sp} of 3800 s for hydrogen fuel and 1500 s for propane. Parametric performance studies show that performance gradually drops with the flight speed, but a Mach number of 5.0 is achievable. Optimal performance is expected to occur at the highest value of Ψ that can be obtained before the isolator flow becomes subsonic. Once the isolator flow is subsonic, an area ratio increase no longer results in a static pressure reduction so matching the average annulus pressure to the inlet pressure cannot be achieved.

Beyond a thermodynamic cycle analysis, the airbreathing RDE operability and potential to either be used by itself or as part of a hybrid propulsion system must be considered. As modeled, the engine is clearly sensitive to the area ratio of the isolation and combustor channels. Due to the high operating frequency, the combustor response will be rapid for a change in inlet conditions. This may mean that holding p_2 equivalent to p_4 will be troublesome if the engine controls itself by varying $A_{\Delta_3}/A_{\Delta_2}$ via a mechanical system. However, as seen in the $A_{\Delta_3}/A_{\Delta_2}$ graphs, it is possible to fix this area ratio and fly along a trajectory where Ψ increases. Operating the RDE may be possible with changing the area ratio or equilibrating pressures with mechanical controls or relief valves, but control systems have not had much chance for development since experimental tests have been of short duration. Since the engine requires supersonic inlet flow as modeled, it is subject to a starting problem similar to a ramjet. With an annular

combustor and fairly steady performance between Mach 1.5–5, the engine may be useful for acceleration to Mach 5 before an aircraft transitions to a scramjet engine. Since the RDE has promise for high power density, it may not take up much space while not in use.

Table 1 shows the minimum diameter for hydrocarbon–air RDEs is greater than one meter, which, combined with a high mass flow rate and a radial exit flow velocity component, could create considerable angular momentum on a vehicle. Hishida et al. have shown a density-averaged radial/axial velocity ratio of less than 3% at the exit plane of their RDE simulation [15]. This low percentage suggests the angular momentum may be manageable with small corrections to the vehicle control system. Multichannel combustors with contra-rotating waves may also be envisioned.

Rocket-mode and airbreathing RDEs require much additional development to show that operation can be initiated consistently and sustained. However, short duration tests as well as CFD results are promising and the results of this study show a stable airbreathing engine is realizable over a range of combustor inlet conditions. If long-duration operation is possible, then the performance characteristics coupled with a potentially high power density may lead to feasible design concepts for high-speed flight applications.

Acknowledgements

Research into this subject for EMB was supported by a U.S. Air Force Research Laboratories summer internship (Air Vehicles Directorate, Design Analysis Methods Branch).

References

[1] J.D. Anderson, Modern Compressible Flow: With Historical Perspective, McGraw–Hill Book Co., New York, 2002.
[2] S. Browne, J. Ziegler, J.E. Shepherd, Numerical solution methods for shock and detonation jump conditions, GALCIT Report FM2006.006, California Institute of Technology, Pasadena CA, August 2008.
[3] T.R.A. Bussing, T.E. Bratkovich, J.B. Hinkley, Practical implementation of pulse detonation engines, in: 33rd AIAA/ASME/SAE/ASEE Joint Propulsion Conference & Exhibit, 1997, AIAA Paper 1997-2748.
[4] F.A. Bykovskii, S.A. Zhdan, E.F. Vedernikov, Continuous spin detonations, J. Propul. Power 22 (6) (2006) 1204–1216.
[5] F.A. Bykovskii, S.A. Zhdan, E.F. Vedernikov, Continuous spin detonation in the regime of self-oscillatory ejection of the oxidizer. 2. Air as an oxidizer, Combust. Explo. Shock 47 (2) (2011) 217–225.
[6] J.A. Camberos, D.J. Moorhouse (Eds.), Exergy Analysis and Design Optimization for Aerospace Vehicles and Systems, Progress in Astronautics and Aeronautics, vol. 238, 2011.
[7] G. Canteins, Etude de la détonation continue rotative—Application à la propulsion, Ph.D. thesis, Université de Poitiers, 2006.
[8] T. Endo, T. Fujiwara, A simplified analysis on a pulse detonation engine model, Trans. Japan Soc. Aero. Space Sci. 44 (146) (2002) 217–222.
[9] W. Fickett, W.C. Davis, Detonation: Theory and Experiment, Dover Publications, Inc., Mineola, NY, 2000.
[10] T. Fujiwara, M. Hishida, J. Kindracki, P. Wolanski, Stabilization of detonation for any incoming Mach numbers, Combust. Explo. Shock 45 (5) (2009) 603–605.
[11] T. Fujiwara, S. Tsuge, Quasi-onedimensional analysis of gaseous free detonations, J. Phys. Soc. Jpn. 33 (1) (1972) 237–241.
[12] D. Goodwin, Cantera: Object-oriented software for reacting flows, http://code.google.com/p/cantera, accessed June 2009.
[13] C.M. Guirao, R. Knystautas, J. Lee, W. Benedick, M. Berman, Hydrogen–air detonations, in: 19th Symp. Int. Combust. Proc., 1982, pp. 583–590.
[14] W.H. Heiser, D.T. Pratt, Hypersonic Airbreathing Propulsion, AIAA Education Series, AIAA, Washington DC, 1994.
[15] M. Hishida, T. Fujiwara, P. Wolanski, Fundamentals of rotating detonations, Shock Waves 19 (1) (2009) 1–10.
[16] K. Kailasanath, Review of propulsion applications of detonation waves, AIAA J. 38 (9) (2000) 1698–1708.
[17] M.J. Kaneshige, Gaseous Detonation Initiation and Stabilization by Hypervelocity Projectiles, Ph.D. thesis, California Institute of Technology, 1999.
[18] M. Kaneshige, J.E. Shepherd, Detonation database, GALCIT Report FM97-8, California Institute of Technology, Pasadena CA, 1997.
[19] J. Kindracki, P. Wolanski, Z. Gut, Experimental research on the rotating detonation in gaseous fuels–oxygen mixtures, Shock Waves 21 (2) (2011) 75–84.
[20] R. Knystautas, C. Guirao, J.H. Lee, A. Sulmistras, Measurement of cell size in hydrocarbon–air mixtures and predictions of critical tube diameter, critical initiation energy, and detonability limits, in: J.A. Bowen, N. Manson, A.K. Oppenheim, R.I. Soloukhin (Eds.), Progress in Astronautics and Aeronautics 94 (1984) 23–37.
[21] J.-L. Li, W. Fan, H. Qiu, C.-J. Yan, Y.-Q. Wang, Preliminary study of a pulse normal detonation wave engine, Aerosp. Sci. Technol. 14 (3) (2010) 161–167.
[22] F.K. Lu, H. Fan, D.R. Wilson, Detonation waves induced by a confined wedge, Aerosp. Sci. Technol. 10 (8) (2006) 679–685.
[23] V.I. Manzhalei, V.V. Mitrofanov, V.A. Subbotin, Measurement of inhomogeneities of a detonation front in gas mixtures at elevated pressures, Combust. Explo. Shock 10 (1) (1974) 89–95.
[24] L. Massa, M. Chauhan, F.K. Lu, Detonation–turbulence interaction, Combust. Flame 158 (9) (2011) 1788–1806.
[25] H. Nakayama, T. Moriya, J. Kasahara, A. Matsuo, Y. Sasamoto, I. Funaki, Stable detonation wave propagation in rectangular-cross-section curved channels, Combust. Flame 159 (2) (2012) 859–869.
[26] J.A. Nicholls, R.E. Cullen, The feasibility of a rotating detonation wave rocket motor, RPL-TDR-64-113, University of Michigan, Ann Arbor MI, April 1964.
[27] J.A. Nicholls, R.E. Cullen, K.W. Ragland, Feasibility studies of a rotating detonation wave rocket motor, J. Spacecraft Rockets 3 (6) (1966) 893–898.
[28] C.A. Nordeen, D. Schwer, F. Schauer, J. Hoke, T. Barber, B. Cetegen, Energy transfer in a rotating detonation engine, in: 47th AIAA/ASME/SAE/ASEE Joint Propulsion Conference & Exhibit, 2011, AIAA Paper 2011-6045.
[29] Z. Pan, B. Fan, X. Zhang, M. Gui, G. Dong, Wavelet pattern and self-sustained mechanism of gaseous detonation rotating in a coaxial cylinder, Combust. Flame 158 (11) (2011) 2220–2228.
[30] R. Petela, Application of exergy analysis to the hydrodynamic theory of detonation in gases, Fuel Process. Technol. 67 (2) (2000) 131–145.
[31] L.A. Povinelli, Impact of dissociation and sensible heat release on pulse detonation and gas turbine engine performance, NASA TM 2001-211080, Cleveland, OH, July 2001.
[32] J.M. Powers, Oblique detonations: Theory and propulsion applications, in: T.L. Jackson, A. Kumar (Eds.), Combustion in High-Speed Flows, Kluwer Academic Publishers, 1994, pp. 345–371.
[33] G.D. Roy, S.M. Frolov, A.A. Borisov, D.W. Netzer, Pulse detonation propulsion: Challenges, current status, and future perspective, Prog. Energ. Combust. 30 (6) (2004) 545–672.
[34] D. Schwer, K. Kailasanath, Numerical investigation of the physics of rotating-detonation-engines, P. Combust. Inst. 33 (2) (2011) 2195–2202.
[35] I. Shen, T.C. Adamson, Theoretical analysis of a rotating two phase detonation in a rocket motor, NASA CR 121194, Ann Arbor MI, March 1973.
[36] M. Sichel, J.C. Foster, The ground impulse generated by a plane fuel–air explosion with side relief, Acta Astronaut. 6 (3–4) (1979) 243–256.
[37] G.P. Smith, D.M. Golden, M. Frenklach, N.W. Moriarty, B. Eiteneer, M. Goldenberg, C.T. Bowman, R.K. Hanson, S. Song, W.C. Gardiner, V.V. Lissianski, Z. Qin, GRI-Mech, http://www.me.berkeley.edu/gri_mech, accessed September 2011.
[38] S. Tsuge, T. Fujiwara, On the propagation velocity of a detonation-shock combined wave, Z. Angew. Math. Mech. 54 (3) (1974) 157–164.
[39] B.V. Voitsekhovskii, Stationary spin detonation, Sov. J. Appl. Mech. Tech. Phys. 3 (1960) 157–164.
[40] Y. Wu, F. Ma, V. Yang, System performance and thermodynamic cycle analysis of airbreathing pulse detonation engines, J. Propul. Power 19 (4) (2003) 556–567.
[41] T.-H. Yi, J. Lou, C. Turangan, J.-Y. Choi, P. Wolanski, Propulsive performance of a continuously rotating detonation engine, J. Propul. Power 27 (1) (2011) 171–181.
[42] S.A. Zhdan, Mathematical model of continuous detonation in an annular combustor with a supersonic flow velocity, Combust. Explo. Shock 44 (6) (2008) 690–697.